Neonatal Enteropathogenic *Escherichia coli* Infection Disrupts Microbiota-Gut-Brain Axis Signaling

Carly Hennessey,[a] Ciara E. Keogh,[a] Mariana Barboza,[a] Ingrid Brust-Mascher,[a] Trina A. Knotts,[b] Jessica A. Sladek,[a] Matteo M. Pusceddu,[a]* Patricia Stokes,[a] Gonzalo Rabasa,[a] Mackenzie Honeycutt,[a] Olivia Walsh,[a] Rene Nichols,[a] [ID]Colin Reardon,[a] [ID]Mélanie G. Gareau[a]

aDepartment of Anatomy, Physiology and Cell Biology, School of Veterinary Medicine, University of California, Davis, Davis, California, USA
bDepartment of Molecular Biosciences, School of Veterinary Medicine, University of California, Davis, Davis, California, USA

ABSTRACT Diarrheal diseases are a leading cause of death in children under the age of 5 years worldwide. Repeated early-life exposures to diarrheal pathogens can result in comorbidities including stunted growth and cognitive deficits, suggesting an impairment in the microbiota-gut-brain (MGB) axis. Neonatal C57BL/6 mice were infected with enteropathogenic *Escherichia coli* (EPEC) (strain e2348/69; Δ*escV* [type III secretion system {T3SS} mutant]) or the vehicle (Luria-Bertani [LB] broth) via oro-gastric gavage at postnatal day 7 (P7). Behavior (novel-object recognition [NOR] task, light/dark [L/D] box, and open-field test [OFT]), intestinal physiology (Ussing chambers), and the gut microbiota (16S Illumina sequencing) were assessed in adulthood (6 to 8 weeks of age). Neonatal infection of mice with EPEC, but not the T3SS mutant, caused ileal inflammation in neonates and impaired recognition memory (NOR task) in adulthood. Cognitive impairments were coupled with increased neurogenesis (Ki67 and doublecortin immunostaining) and neuroinflammation (increased microglia activation [Iba1]) in adulthood. Intestinal pathophysiology in adult mice was characterized by increased secretory state (short-circuit current [I_{sc}]) and permeability (conductance) (fluorescein isothiocyanate [FITC]-dextran flux) in the ileum and colon of neonatally EPEC-infected mice, along with increased expression of proinflammatory cytokines (*Tnfα*, *Il12*, and *Il6*) and pattern recognition receptors (*Nod1/2* and *Tlr2/4*). Finally, neonatal EPEC infection caused significant dysbiosis of the gut microbiota, including decreased *Firmicutes*, in adulthood. Together, these findings demonstrate that infection in early life can significantly impair the MGB axis in adulthood.

KEYWORDS microbiota-gut-brain axis, behavior, neuroinflammation, neurogenesis, bacterial infection

D espite advances in sanitation and access to clean drinking water, enteric infections remain a global public health issue, with diarrheal diseases being a leading cause of death in children under the age of 5 years worldwide (1). While treatment of diarrhea with an oral rehydration solution has significantly decreased childhood mortality, repeated exposures to diarrheal pathogens have been correlated with impaired growth and cognitive deficits into adulthood (2–4). Malnutrition caused by enteric bacterial pathogens may support ongoing dysbiosis, resulting in gastrointestinal (GI) barrier dysfunction and systemic translocation of bacterial products (3, 5). This translocation may drive systemic inflammation, and neuroinflammation, which could contribute to cognitive deficits. Despite this association, the underlying cause of enteric infection-induced cognitive deficits is unknown.

Early neonatal life is a critical time for neural development (6), differentiation and maturation of the GI tract (7), and colonization of the gut microbiota (8), together comprising the microbiota-gut-brain (MGB) axis. Signaling of the MGB axis occurs via hormones,

A. Experimental timeline

B. EPEC Colonization

FIG 1 Study design and EPEC colonization. (A) Mouse pups were challenged at P7 (EPEC, $\Delta escV$, or LB broth [sham]), and adults were divided into 3 experimental groups. (B) Colonic (left) and ileum (right) samples grown on MacConkey agar plates at 1, 4, 8, and 12 days postinfection to quantify EPEC and $\Delta escV$ colonization. Data represent 1 to 2 pups per litter from 3 to 4 separate litters per group per time point.

neurotransmitters, and immune cells, although the precise pathways involved remain to be fully elucidated (9, 10). Dysbiosis, induced following either antibiotic administration (11) or infection with a bacterial pathogen (12), can result in long-lasting impairments in MGB axis signaling, including behavioral 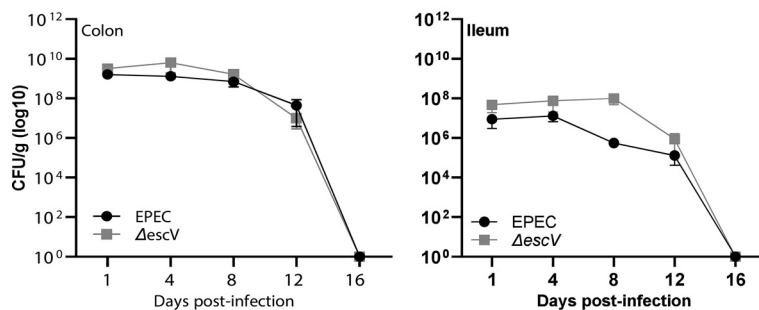deficits and GI pathophysiology. For example, in adult mice, infection with the murine bacterial pathogen *Citrobacter rodentium* causes acute anxiety-like behavior (13) and stress-induced cognitive deficits (12), with exposure to social stress increasing the severity of infection (14). These studies highlight the association between infection, dysbiosis, inflammation, and behavioral impairments, which may be further enhanced following initiation during early neonatal life.

Here, we sought to identify the effects of neonatal bacterial enteric infection on the MGB axis by infecting mouse pups with enteropathogenic *Escherichia coli* (EPEC). While EPEC does not colonize adult mice without antibiotic pretreatment (15), it can effectively colonize both the ileum and colon in neonatal mice (16). Epithelial cell attachment and EPEC microcolony formation depend on the presence of functional bundle-forming pili and the type III secretion system (T3SS) (16). This molecular syringe permits the injection of virulence factors into the host cell and triggers inflammatory responses to infection. Following neonatal EPEC infection, we identified recognition memory deficits, GI pathophysiology, and dysbiosis in adult mice. These MGB axis defects were coupled with increased hippocampal neurogenesis and neuroinflammation, identifying a potential novel pathway through which neonatal enteric bacterial infection can cause cognitive deficits in adulthood.

RESULTS

EPEC colonizes neonatal mice and leads to GI inflammation. Mice were infected with EPEC or $\Delta escV$ at postnatal day 7 (P7) and colonization assessed over time until weaning (P21) (Fig. 1A). EPEC and $\Delta escV$ both effectively colonized mice, as demonstrated by increased CFU per gram of tissue, reaching 10^8 to 10^9 CFU/g tissue (colon) and 10^6 to 10^7 CFU/g tissue (ileum) by 1 to 4 days postinfection (p.i.), and reduced bacterial burden starting at 12 days p.i., with all mice clearing the bacteria by 16 days p.i. (Fig. 1B). An absence of overt histological damage was observed in the ileum of EPEC- or
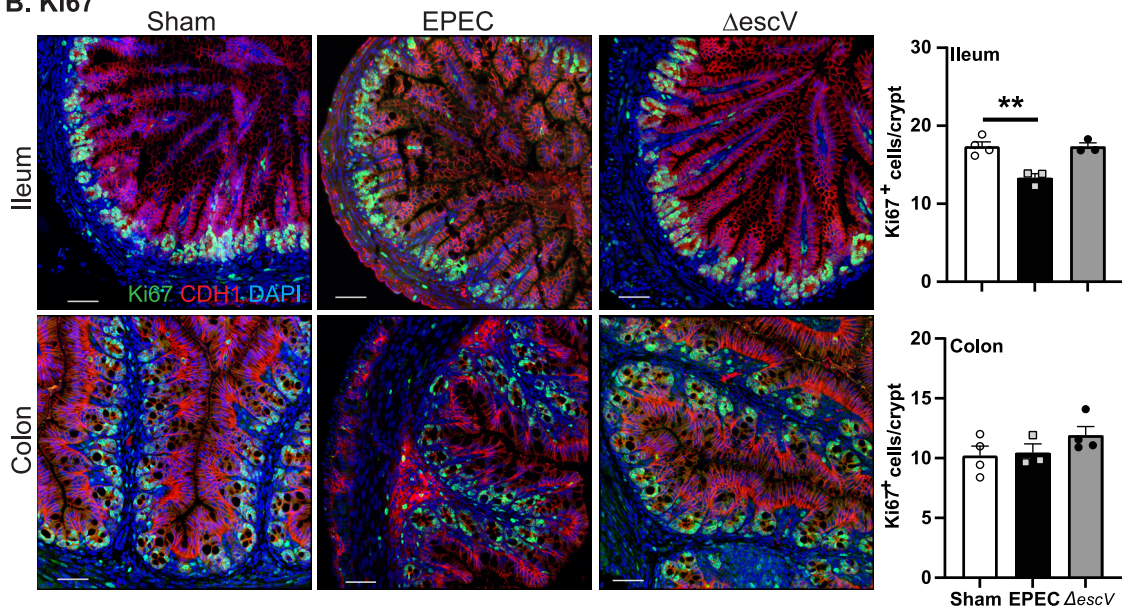
A. Histology
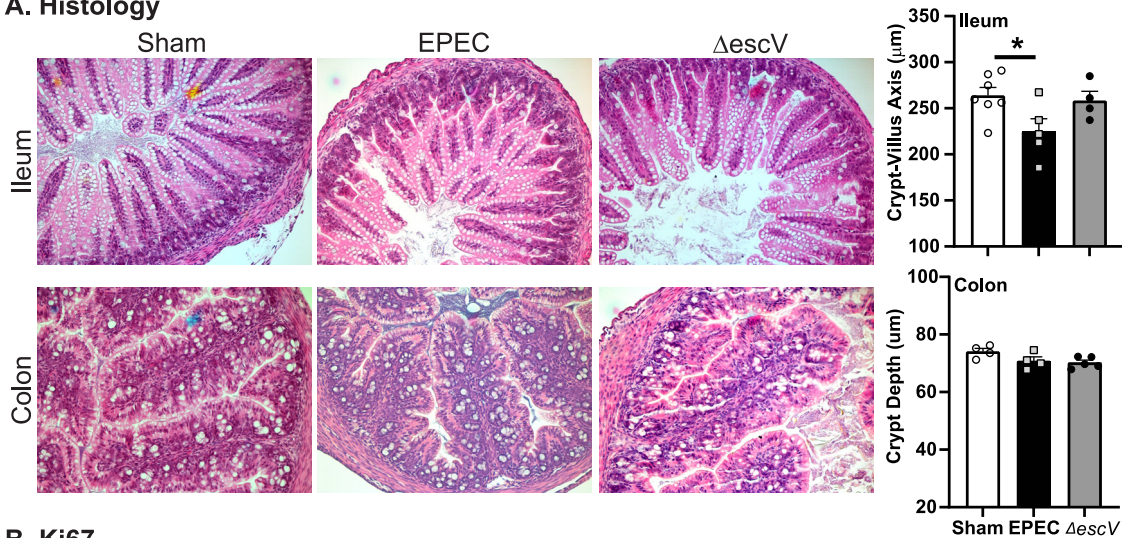
B. Ki67

FIG 2 Neonatal GI histology. (A) Representative histological images (H&E staining) of ileum and colon from sham-, EPEC-, and ΔescV-challenged mice at 7 days postinfection (left) and quantification of the crypt-villus axis (ileum) and crypt depth (colon) (right). (B) Representative images of epithelial cell proliferation assessment by Ki67 (proliferation marker) (green), CDH1 (epithelial cell marker) (red), and DAPI (nuclei) (blue) in the ileum and colon (left) and quantification of cell numbers (right) ($n = 3$ to 5 mice per group) (*, $P \leq 0.05$; **, $P \leq 0.01$ [by one-way ANOVA and Tukey's *post hoc* test]). Bars = 100 μm.

ΔescV-infected mice at 7 days p.i. (Fig. 2A). Despite the lack of obvious damage, characterization of the crypt-villus axis in the ileum identified a significant shortening in length in EPEC-infected mice compared to sham- or ΔescV-infected mice (Fig. 2A). This shortening in the ileum was coupled with a decrease in epithelial cell proliferation, indicated by decreased numbers of Ki67-positive (Ki67+) cells (Fig. 2B). In contrast, no damage, change in crypt depth, or impact on epithelial cell proliferation was found in the colon (Fig. 2A and B). These results indicate that EPEC infection of neonatal mice causes ileal damage in a T3SS-dependent manner.

In order to further support histological findings, the expression of cytokines and pattern recognition receptors (PRRs) was assessed in the ileum and colon by quantitative PCR (qPCR). The expression of *Il1β*, *Il10*, *Il12*, and *Tnfα* was significantly increased in the ileum of EPEC-infected versus sham-infected mice at P14 (7 days p.i.) but absent in ΔescV-infected mice (Fig. 3A). In the colon, immune activation was limited in EPEC-infected mice,
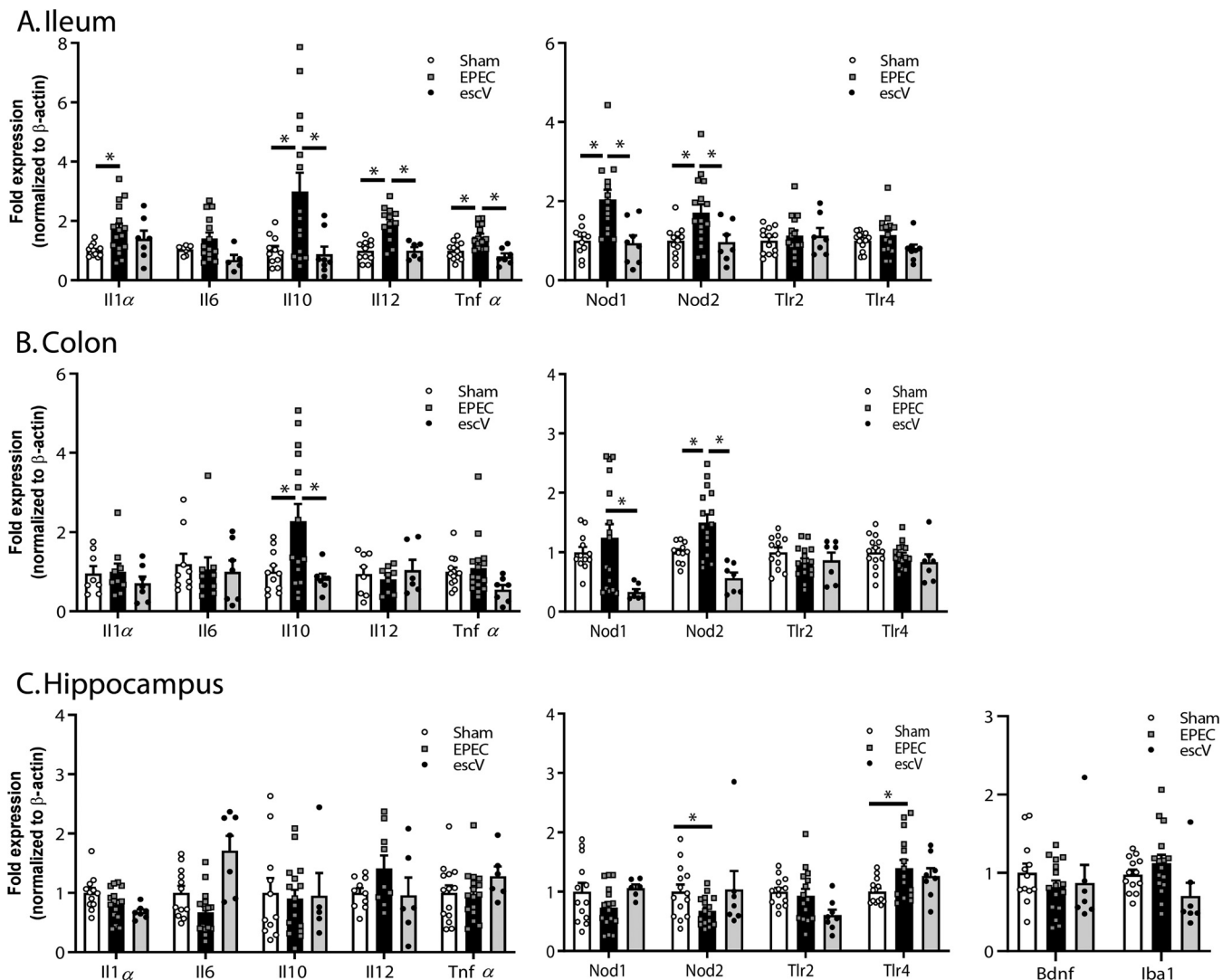
A. Ileum

B. Colon

C. Hippocampus

FIG 3 Neonatal GI inflammation. Relative mRNA expression levels in the ileum (A), colon (B), and hippocampus (C) at P14 are shown for cytokines and pattern recognition receptors ($n = 8$ to 16 mice per group) (*, $P \leq 0.05$ [by one-way ANOVA and Tukey's *post hoc* test]).

with only *Il10* expression being significantly increased (Fig. 3B), while no evidence of immune activation was seen in the hippocampus (Fig. 3C). Infection also significantly increased the expression of the PRRs *Nod1* and *Nod2* in the ileum and *Nod2* in the colon, whereas in the hippocampus, EPEC infection reduced *Nod2* expression and increased *Tlr4* (Fig. 3A to C). Inflammation was dampened by P21, with only *Il1β* in the ileum and *Il6*, *Il10*, and *Tnfα* in the colon being elevated as the bacterial burden decreased (see Fig. S1 in the supplemental material). In the hippocampus, elevated levels of *Il1β* and *Il6* were seen, along with increased expression of the microglia marker *Iba1* (Fig. S1), suggesting ongoing mild immune activation at P21 in both the gut and the brain.

Neonatal EPEC infection causes cognitive deficits in adulthood. To study the impact of neonatal EPEC infection on the MGB axis in adulthood, behavioral testing was performed. Recognition memory (novel-object recognition [NOR] task) was impaired in EPEC-infected mice versus sham-infected controls, as indicated by a decreased exploration ratio (Fig. 4A). This effect was dependent on infection via the T3SS, as recognition memory was unaffected in mice infected with the ΔescV mutant strain (Fig. 4A). In contrast, EPEC infection did not impact anxiety-like behavior (light/ dark [L/D] box), with time spent in the light and transitions between the light and dark boxes being similar among sham-, EPEC-, and ΔescV-infected groups (Fig. 4B).
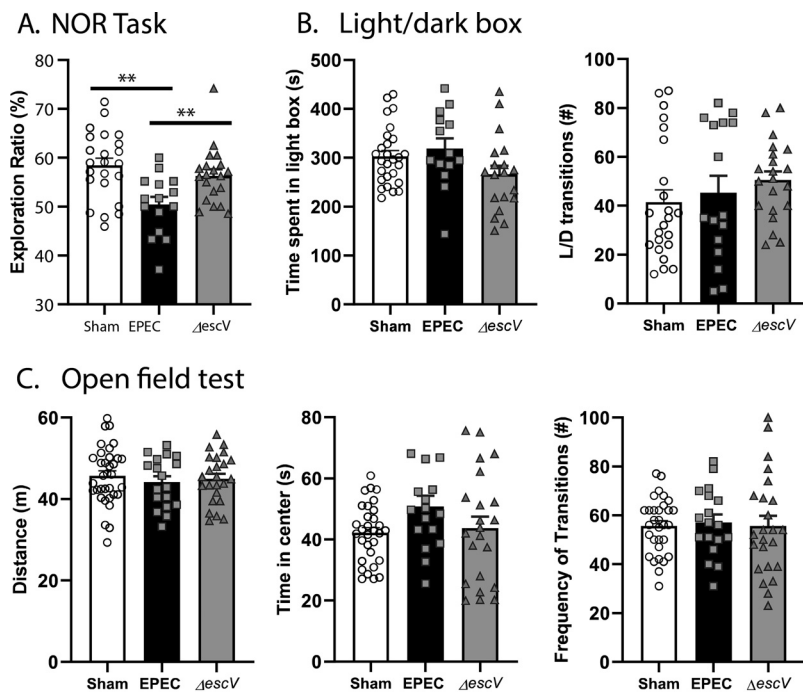
FIG 4 Neonatal EPEC infection induces cognitive deficits in adulthood. (A) Recognition memory was assessed using the novel-object recognition (NOR) task by quantification of the exploration ratio (percent). (B) Anxiety-like behavior was assessed using the light/dark (L/D) box by measuring the time spent in the light box and transitions between the light and dark boxes. (C) General locomotor activity was determined using the open-field test (OFT), by measuring the total distance traveled, frequency of transitions to the inner zone, and time spent in the inner zone ($n = 15$ to 34 mice per group) (***, $P < 0.001$ [by one-way ANOVA and Holm-Sidak's *post hoc* test]).

Locomotor activity (open-field test [OFT]) was also normal, with total distance traveled, frequency of transitions, and time spent in the center of the arena being the same in EPEC-infected mice and sham-treated controls (Fig. 4C). These findings suggest that neonatal EPEC infection causes recognition memory deficits in adulthood in a T3SS-dependent manner, without inducing anxiety-like behavior or reducing locomotor activity.

Neonatal EPEC infection increases hippocampal neurogenesis in adult mice. As the primary site of adult neurogenesis, the dentate gyrus (DG) region of the hippocampus plays a critical role in hippocampal plasticity (17), learning, and memory (18). Immature neurons (doublecortin-positive [DCX$^+$] neurons per cubic micrometer [*, $P < 0.05$]) and proliferating cells (Ki67$^+$ cells per cubic micrometer [*, $P < 0.05$]) were significantly increased in the DG of EPEC-infected mice versus sham-infected controls (Fig. 5A and B). Increased neurogenesis in EPEC-infected mice was associated with increased expression of brain-derived neurotrophic factor (BDNF), critical for supporting neuronal growth and neurogenesis (18) (Fig. 5C). Taken together, these findings suggest that neonatal EPEC infection increased hippocampal neurogenesis in adulthood.

Neonatal EPEC infection causes neuroinflammation and microglia activation in adulthood. Neurogenesis can be detrimentally impacted by the presence of neuroinflammation. Since neonatal EPEC infection reduced recognition memory and increased hippocampal neurogenesis in adulthood, neuroinflammation was assessed by qPCR. Although levels of hippocampal expression of *Il10* and *Il22* were both increased, no change was observed in *Il1β*, *Il6*, or *Tnfα* in adult mice neonatally infected with EPEC. Increased expression of several PRRs (*Nod1*, *Nod2*, and *Tlr2*) was also observed, along with increased expression of the microglia marker *Iba1*, in adult EPEC mice, suggesting immune activation (Fig. 6A). This was specific to the hippocampus, with the cerebellum and prefrontal cortex (PFC) region showing little evidence of immune activation (Fig. S2).
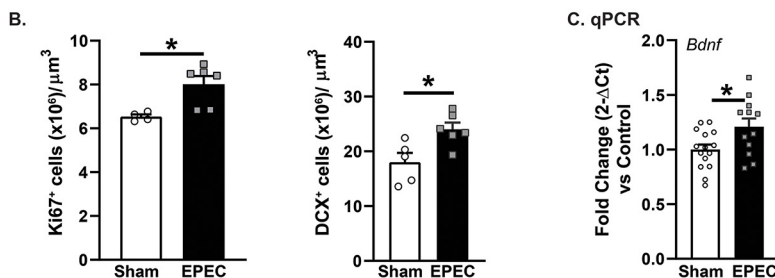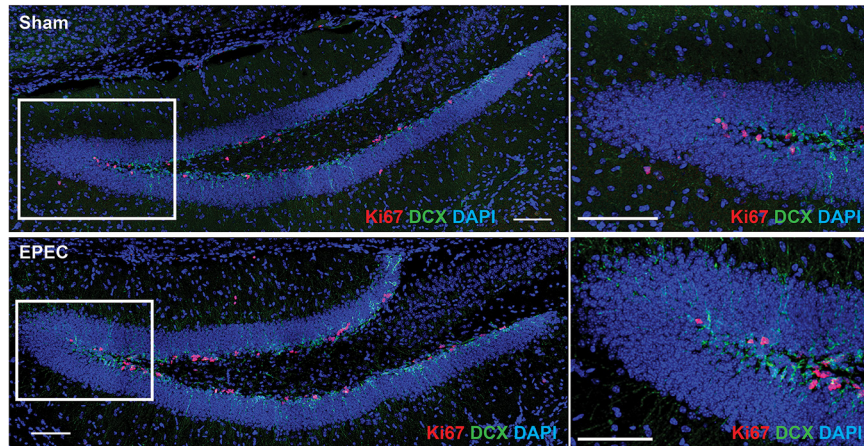
A. Ki67 and DCX

B.

C. qPCR

FIG 5 Neonatal EPEC infection impairs hippocampal neurogenesis in adulthood. (A) Confocal imaging was used to assess neurogenesis via quantification of cell proliferation (Ki67) (red) and immature neurons (doublecortin [DCX]) (green). Bars = $100\,\mu$m. (B) Quantification of Ki67$^+$ and DCX$^+$ cells per cubic micrometer in the dentate gyrus (DG) ($n = 5$ mice per group) (*, $P \leq 0.05$ [by Student's t test]). (C) Relative mRNA expression of $Bdnf$ in the hippocampus ($n = 16$ mice per group) (*, $P \leq 0.05$ [by Student's t test]).

Microglia are resident immune cells in the brain, with their activation regulated in part by the gut microbiota (19, 20). Upon activation, microglia retract their processes becoming more amoeboid, changing their morphology (20). Hippocampal microglia in EPEC-infected mice had a more activated phenotype, characterized by significantly decreased process lengths, decreased numbers of branch points, and reduced numbers of terminal points in the DG and cornu ammonis 1 (CA1) regions, coupled with increased cell numbers (Fig. 6B). Taken together, these findings support the activation of microglia in the adult hippocampus following neonatal EPEC infection.

Neonatal EPEC infection results in intestinal pathophysiology in adulthood. Diarrheal disease is caused by an imbalance between secretory and absorptive functions of the intestinal epithelium, often coupled with impaired permeability (21). Neonatal EPEC infection increased baseline ileal and colonic ion transport (short-circuit current [I_{sc}]) compared to sham-infected controls (Fig. 7A). Increased permeability was also demonstrated in neonatally EPEC-infected mice by elevated conductance (G) (Fig. 7B) and fluorescein isothiocyanate (FITC)-dextran flux (Fig. 7C) in both the ileum and colon, indicating increased tight junction and macromolecular permeability, respectively. No obvious histopathology was observed, suggesting the absence of overt damage in either the ileum or colon (Fig. 7D). Despite the absence of microscopic damage, neonatal EPEC infection increased the expression of proinflammatory cytokines ($Il6$, $Il22$, and $Tnf\alpha$), PRRs ($Nod1$, $Nod2$, $Tlr2$, and $Tlr4$), $RegIII\gamma$, and $Bdnf$ in the ileum (Fig. 7E) and increased the expression of $Tlr2$ in the colon in adult mice. Therefore, while neonatal EPEC infection leads to impaired mucosal barrier function in the adult ileum and colon, evidence of mild immune activation was observed only in the ileum.

Neonatal EPEC infection causes long-lasting changes to the gut microbiota. In order to characterize changes to the gut microbiota following neonatal EPEC infection,

A. qPCR Hippocampus
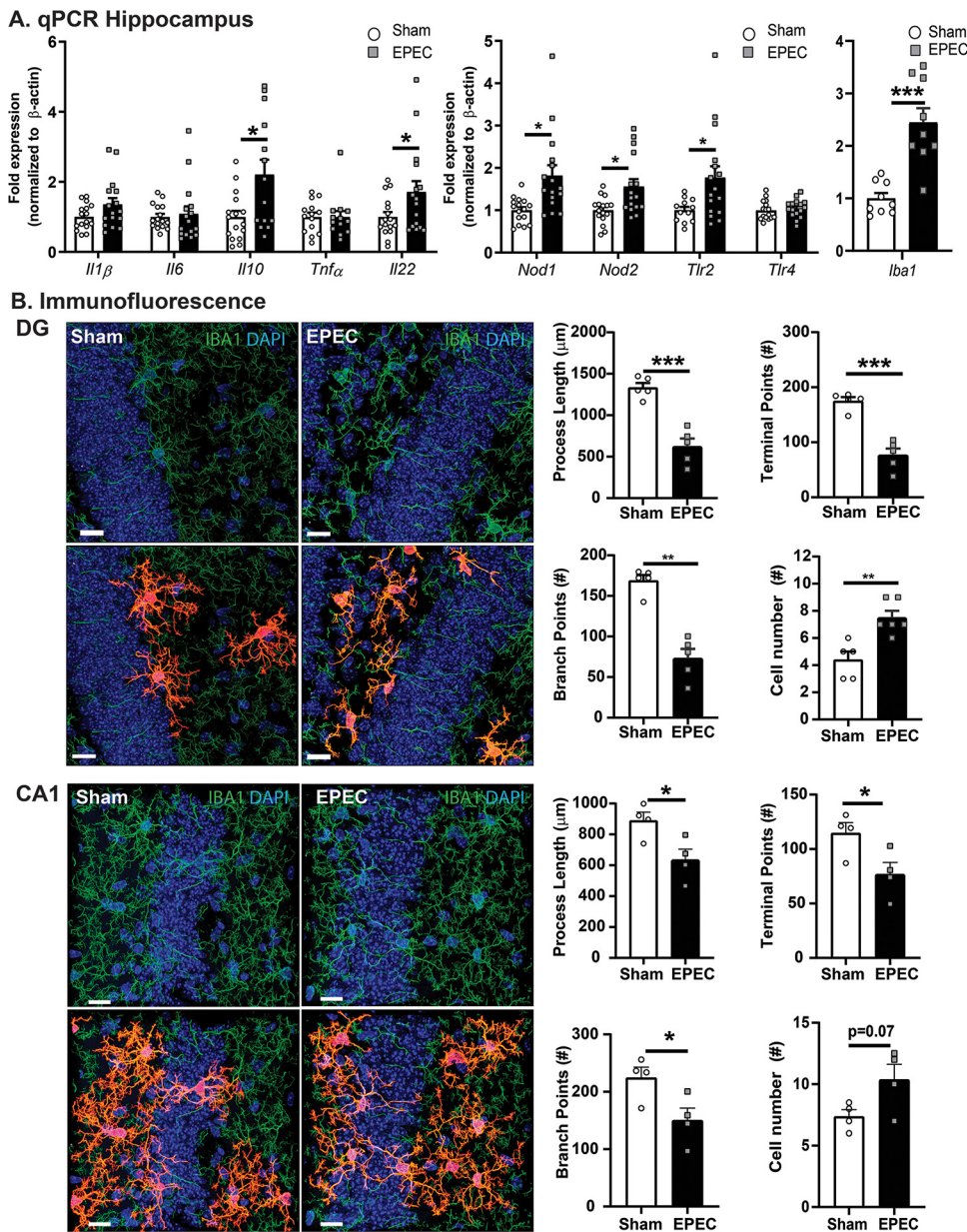

B. Immunofluorescence

DG

CA1

FIG 6 Neonatal EPEC infection increases hippocampal neuroinflammation in adulthood. (A) Relative mRNA expression in the hippocampus ($n = 12$ to 16 mice per group) (*, $P \leq 0.05$; **, $P \leq 0.01$ [by Student's t test, with a Mann-Whitney test and Welch's correction where appropriate]). (B) Confocal imaging and morphological characterization of microglia in the dentate gyrus (DG) (top) and CA1 region (bottom) of the hippocampus. (Left) Microglia (Iba1) (green) with single-cell overlays (red) identified with 3DMorph and morphology characterized using Imaris. (Right) Process lengths, terminal points, branch points, and cell numbers were quantified. Nuclei were stained with DAPI ($n = 5$ to 6 mice per group) (**, $P < 0.01$; ***, $P < 0.001$ [by Student's t test]). Bars = 15 μm.

16S rRNA sequencing of fecal samples from 6- to 8-week-old mice was performed. The Shannon and Chao1 indices suggest a trend toward decreased alpha diversity in neonatally EPEC-infected mice compared to sham-infected controls (Shannon index P value of 0.09 and Chao1 index P value of 0.07 by a Kruskal-Wallis pairwise comparison) (Fig. 8A). Using genus-level abundance, partial least-squares discriminant analysis (PLS-DA) showed that adult sham- and EPEC-infected mice formed separate and distinct clusters (Fig. 8B). Phylum-level abundances show marked increases in *Actinobacteria* and decreased *Firmicutes* following neonatal EPEC infection compared to sham-infected
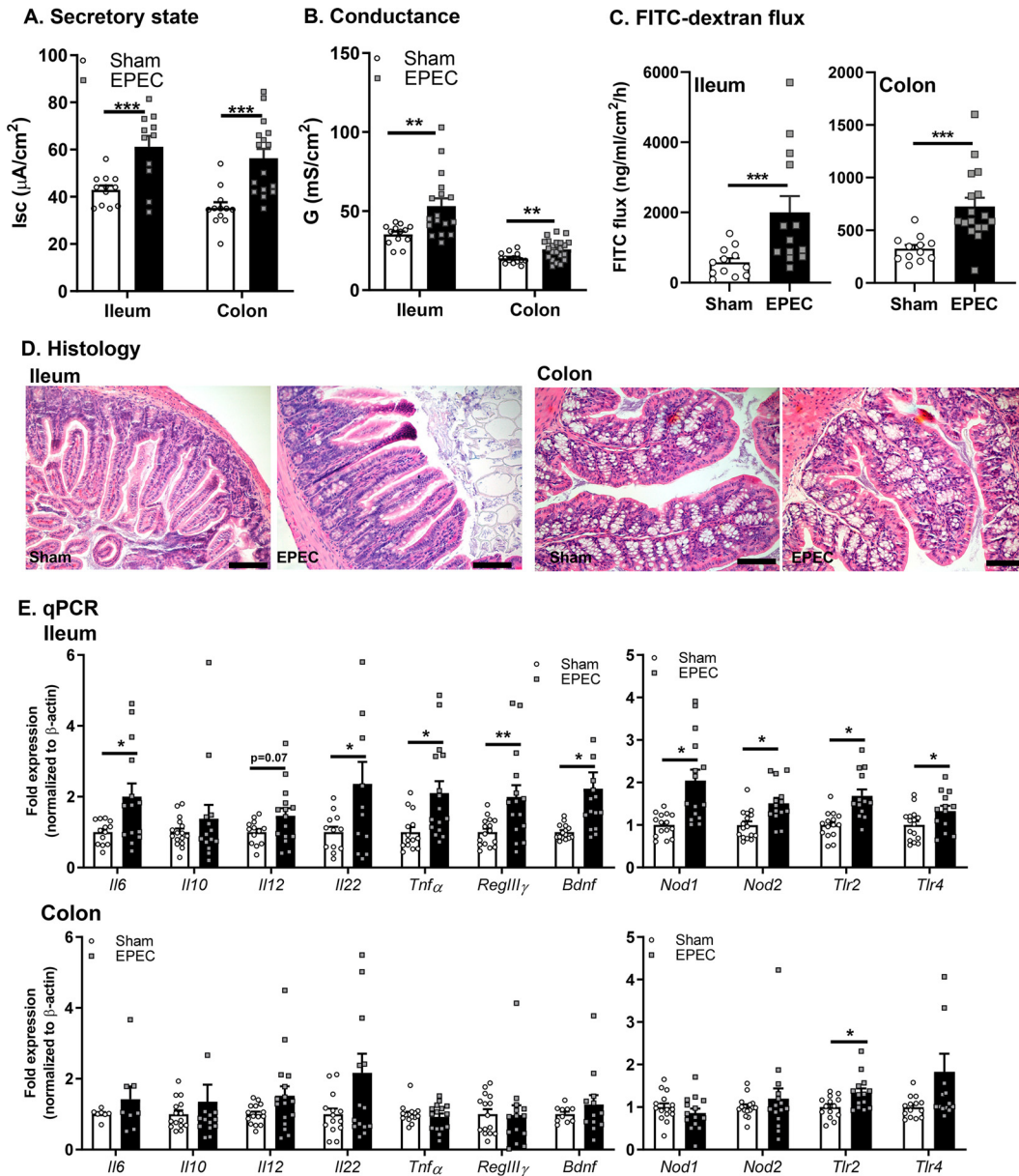
FIG 7 Neonatal EPEC infection caused impaired intestinal physiology in adulthood. (A to C) Ussing chambers were used to assess the secretory state (short-circuit current [I_{sc}]) (A) and tight junction permeability via conductance (*G*) (B) and FITC-dextran flux (C) in both the ileum and colon. (D) Histology of ileum (left) and colon (right) with representative H&E staining. (E) Relative mRNA expression in the ileum and colon ($n = 12$ to 16 mice per group) (*, $P \leq 0.05$; **, $P \leq 0.01$; ***, $P < 0.001$ [by Student's *t* test, with a Mann-Whitney test and Welch's correction where appropriate]).

controls (Fig. 8C). At the family level, several members of the *Lachnospiraceae* and *Ruminococcaceae* families were decreased in EPEC-infected mice (Fig. 8D), whereas *Lactobacillaceae* and *Bifidobacteriaceae* were significantly increased (Fig. 8D). Taken together, these findings suggest that neonatal EPEC infection impairs the colonization of the gut microbiota, with persistent dysbiosis in adulthood.

DISCUSSION

Given that the establishment of the MGB axis occurs in early life, neonatal enteric infections can potentially have long-lasting effects on microbiota composition, intestinal physiology, the brain, and behavior. Here, we demonstrate for the first time that neonatal EPEC infection can have lasting adverse effects on the MGB axis in mice, well

A. Alpha diversity
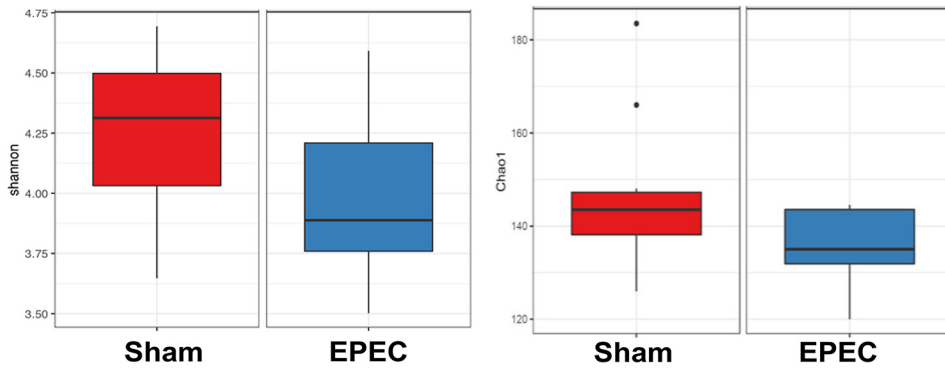
B. PLS-DA

C. Phylum level abundances

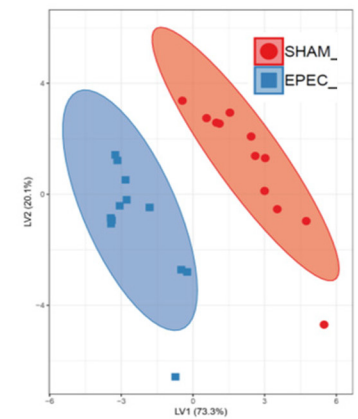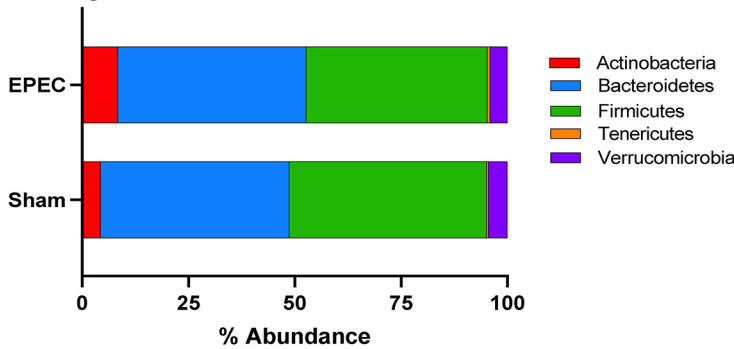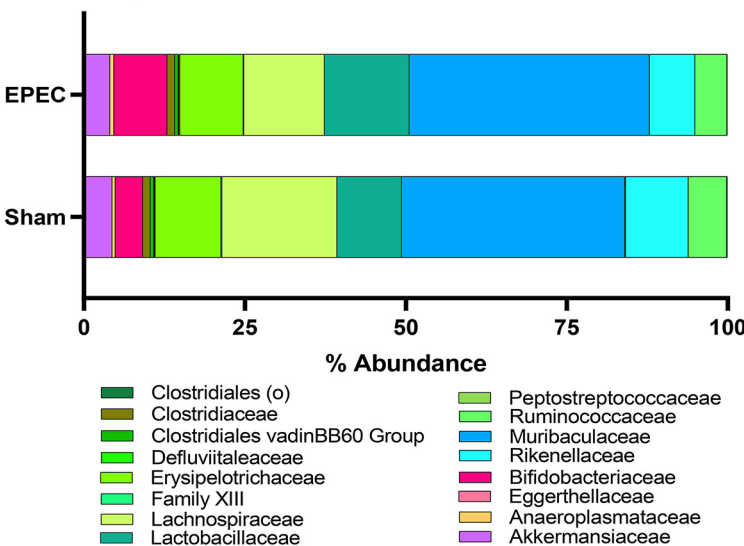|	Sham	EPEC	P value
Actinobacteria	4.36 ± 1.72	8.39 ± 2.23	***
Bacteroidetes	44.4 ± 2.55	44.33 ± 2.8	
Firmicutes	46.31 ± 1.82	42.57 ± 1.81	***
Tenericutes	0.54 ± 0.18	0.67 ± 0.21	
Verrucomicrobia	4.39 ± 0.8	4.04 ± 0.62	

Legend: ■ Actinobacteria ■ Bacteroidetes ■ Firmicutes ■ Tenericutes ■ Verrucomicrobia

D. Family level abundances

	Sham	EPEC	P value
Akkermansiaceae	4.39 ± 0.8	4.04 ± 0.62	
Anaeroplasmataceae	0.49 ± 0.18	0.63 ± 0.21	
Bifidobacteriaceae	4.27 ± 1.71	8.25 ± 2.23	***
Clostridiaceae	1.17 ± 0.57	1.19 ± 0.43	
Clostridiales	0.56 ± 0.13	0.57 ± 0.11	
Defluviitaleaceae	0.1 ± 0.02	0.1 ± 0.03	
Eggerthellaceae	0.1 ± 0.01	0.14 ± 0.02	***
Erysipelotrichaceae	10.22 ± 1.42	9.83 ± 2.23	
Family XIII	0.17 ± 0.02	0.13 ± 0.02	***
Lachnospiraceae	17.87 ± 2.29	12.51 ± 2.34	***
Lactobacillaceae	10.03 ± 1.54	13.17 ± 1.85	***
Muribaculaceae	34.64 ± 2.02	37.31 ± 2.49	
Peptostreptococcaceae	0.14 ± 0.05	0.02 ± 0.01	***
Rikenellaceae	9.76 ± 1.11	7.01 ± 0.9	***
Ruminococcaceae	5.96 ± 0.55	4.99 ± 0.46	***
Clostridiales (o)	0.06 ± 0.02	0.05 ± 0.02	

Legend:
■ Clostridiales (o) ■ Clostridiaceae ■ Clostridiales vadinBB60 Group ■ Defluviitaleaceae ■ Erysipelotrichaceae ■ Family XIII ■ Lachnospiraceae ■ Lactobacillaceae ■ Peptostreptococcaceae ■ Ruminococcaceae ■ Muribaculaceae ■ Rikenellaceae ■ Bifidobacteriaceae ■ Eggerthellaceae ■ Anaeroplasmataceae ■ Akkermansiaceae

FIG 8 Dysbiosis in adult mice following neonatal EPEC infection. 16S rRNA Illumina sequencing was performed on fecal pellets to characterize the microbiota. (A) Shannon and Chao1 measures of alpha diversity. (B) Multivariate analysis using partial least-squares discriminant analysis (PLS-DA) of genus-level abundances. (C and D) Phylum-level (C) and family-level (D) abundances, with the highest-abundance species presented and statistics outlined in the tables ($n = 12$ mice per group) (***, $P < 0.001$ [by a Holm-Sidak test]).

past the resolution of infection. Adult mice neonatally infected with EPEC exhibited cognitive deficits, increased neurogenesis, neuroinflammation, intestinal pathophysiology, and altered gut microbiota composition compared to sham-infected controls. These adverse effects appear to be pathogen associated, as neonatal intestinal inflammation and behavioral impairments in adulthood were absent in mice infected with a

T3SS mutant strain. Our findings have implications for better understanding the long-term consequences of enteric infections in early life and other diarrheal diseases in humans.

Multiple studies in adult germfree (12, 22, 23), antibiotic-treated (24, 25), or bacterially infected (12, 26) mice have established that changes to the gut microbiota significantly affect the brain and behavior. In developmental studies, maternal antibiotic administration resulted in dysbiosis, coupled with anxiety-like behavior and social behavioral deficits in the pups (11). Similarly, early-life stress induced by maternal separation leads to intestinal dysbiosis and pathophysiology (27) as well as behavioral deficits, including despair and anxiety-like behavior (28). Here, we found that neonatal infection with a bacterial pathogen led to cognitive deficits without causing anxiety-like behavior in adulthood. These EPEC-induced cognitive deficits required bacterial virulence factors as mice infected with the avirulent $\Delta escV$ EPEC strain did not induce memory deficits. These findings indicate that altered host behaviors are due to active infection and not simply due to Enterobacteriaceae colonization. Additionally, these findings suggest that impaired host-microbe interactions caused by a bacterial pathogen in early life can disrupt cognitive function in adulthood.

Neurogenesis is important for maintaining hippocampus-dependent cognitive function, with perturbations seen in neurodegenerative disorders (29). Early-life experiences, particularly exposure to stress, can impair the rate of adult hippocampal neurogenesis as demonstrated by decreases in cell proliferation and immature neuron production in the DG of adult rats that are maternally separated as pups (30). In addition, germfree mice have increased hippocampal neurogenesis in adulthood, suggesting a role for the microbiota in the regulation of this process (31). In our studies, neonatal EPEC infection increased hippocampal BDNF expression and the numbers of proliferating cells and immature neurons, suggesting an increase in neurogenesis. Given the importance of neurogenesis in memory formation and retention, increased hippocampal neurogenesis could in part explain the recognition memory deficits observed in neonatally EPEC-infected adult mice.

Neuroinflammation occurs in numerous behavioral and cognitive disorders, with microglia activation implicated in the onset and progression of neurodevelopmental and neurodegenerative diseases (20). These resident immune cells of the brain survey their microenvironment and are essential for the phagocytosis of dying cells; additionally, they play an important role in the regulation of neurogenesis and can induce synaptic remodeling (20). Systemic injection of nonpathogenic E. coli in neonatal rats caused microglial activation, impaired neurogenesis, and behavior deficits following subsequent immune challenge with lipopolysaccharide in adulthood (32). Similarly, we identified adult memory deficits in neonatally EPEC-infected mice that coincide with long-term neuroinflammation, characterized by immune activation, including increased hippocampal cytokines, and increased hippocampal microglia numbers and morphology representing activation. Taken together, these findings reinforce the susceptibility of the developing neonatal brain to the MGB axis, with defects that persist until adulthood.

Enteric bacterial pathogens are a major cause of diarrhea in humans, resulting in disease in part due to increased ion transport, driving water efflux to flush away the pathogen from the epithelium. Chronic diarrheal illness is associated with a combination of blunted villi, intestinal barrier dysfunction, and submucosal inflammation (33). In addition, early-life enteric infections that impair intestinal barrier function have been proposed to cause a shift in the gut microbiota, promoting chronic systemic inflammation and, consequently, impaired cognitive development (3). In our studies, neonatal EPEC infection resulted in intestinal pathophysiology, with increased ileal and colonic ion secretion persisting until adulthood. This prosecretory state was associated with increased permeability, suggesting an increased potential for the translocation of bacteria and bacterial products. Indeed, gene expression studies identified increases in many immune-related targets in the ileum of EPEC-infected mice, including *Il6*, *Tnfα*,

RegIIIγ, *Nod1*, *Nod2*, *Tlr2*, and *Tlr4*, which suggests chronic, low-grade ileal inflammation. These results are in keeping with findings in children hospitalized with noncritical infections who have increased intestinal permeability and altered innate immune responses, which potentially increase their risk of subsequent infections (34). This suggests that neonatal bacterial infection can impair the establishment of intestinal mucosal barrier function, leading to a chronic mild inflammatory state.

Colonization of the GI tract by the microbiota is crucial for the establishment of the intestinal epithelial barrier, maintenance of the mucosal immune response, and resistance to pathogens. The dynamic composition of the microbiota in early life makes it more susceptible to dysbiosis. Here, we found that neonatal infection with EPEC decreased the abundance of *Firmicutes*, particularly the *Lachnospiraceae* family, in adult mice. Given the role of *Lachnospiraceae* in short-chain fatty acid production, including butyrate and acetate, decreases in colonization may detrimentally impact host-microbe interactions. Decreased *Lachnospiraceae* were also found in mice exposed to early-life stress that exhibited impaired social behavior (35), suggesting that these bacteria aid in maintaining gut-brain communication. Taken together, these findings highlight the critical role of neonatal colonization in maintaining host-microbe interactions and suggest that restoration of *Lachnospiraceae* levels may be beneficial for gut-brain axis deficits.

In conclusion, neonatal EPEC infection leads to disruption of the MGB axis, characterized by cognitive deficits, neuroinflammation, intestinal pathophysiology, and gut dysbiosis in adulthood, via the T3SS. Future studies will serve to determine the directionality of these effects, for example, whether neonatal EPEC-induced dysbiosis leads to gut pathophysiology and subsequent neuroinflammation in adulthood or whether these effects occur independently of one another. Given the correlation between enteric bacterial infection in children and cognitive function in adulthood, these studies highlight the impact that enteric infections can have on the MGB axis and the importance of reestablishing signaling in early life to prevent persistent impairments in adulthood. Future studies assessing the role of beneficial bacteria in ameliorating enteric bacterial infection-induced MGB axis deficits in neonates are therefore highly warranted.

MATERIALS AND METHODS

Mice. Mice (male and female C57BL/6J; originally from Jackson Laboratories) were bred in-house. Mice were housed in cages lined with cob bedding, exposed to a 12-h light/dark cycle, and had access to food and water *ad libitum*. Mice were euthanized by CO_2 followed by cervical dislocation. All procedures and protocols were approved by UC Davis (IACUC number 21862).

Study design. Neonatal mice were challenged on postnatal day 7 (P7) with 50 μl of EPEC (O127:H6 strain E2348/69 or a T3SS mutant [Δ*escV* {kindly provided by Andreas Bäumler}] at 10^5 CFU) or a vehicle (Luria-Bertani [LB] broth) (sham-infected mice) via orogastric gavage (Fig. 1A). Bacteria were grown overnight in LB broth at 37°C and subcultured for 3 h prior to infection. Adult mice (6 to 8 weeks of age) were used for three sets of experiments:

1. Behavioral testing. Mice were acclimated to the testing room overnight. Behavior was assessed between 9:00 a.m. and 4:00 p.m. during the light cycle, with tests performed from least to most stressful: L/D box, OFT, and NOR task. This strategy prevents carryover effects between tests (36). Tissues (hippocampus, cerebellum, PFC region, distal ileum, and proximal colon) were collected for qPCR. Fecal samples were collected for 16S rRNA Illumina sequencing.

2. GI pathophysiology. The distal ileum and proximal colon were collected for Ussing chamber studies. Mice were euthanized, and tissues were immediately collected and placed in ice-cold Ringer's buffer. Additional ileum and colon tissue samples were collected for histology.

3. Neuroinflammation and neurogenesis. Mice were anesthetized with isoflurane (5%) and perfused with 4% paraformaldehyde (PFA), and brains were collected and processed for immunofluorescence.

EPEC colonization. To monitor EPEC or Δ*escV* infection, bacterial colonization was assessed at 1, 4, 8, and 12 days p.i. in 3 to 4 separate litters per group. Distal ileum and proximal colon samples (tissue plus luminal contents/fecal pellets) were weighed, homogenized, serially diluted (10^{-1} to 10^{-6}) for plating on MacConkey agar, and incubated at 37°C overnight. Fecal pellets were collected and plated between P21 and P23 to confirm clearance of the pathogen in all litters. An absence of growth was found in sham-infected controls, confirming that all colonies seen from EPEC/Δ*escV*-challenged mice represent EPEC/Δ*escV* and not commensal *E. coli*. Data are presented as CFU per gram of tissue.

Behavior tests. (i) L/D box. Anxiety-like behavior was assessed using the L/D box test (36–38). Briefly, mice were placed in a novel arena (40 by 20 cm) divided into a dark compartment (1/3) and a light compartment (2/3) and allowed to explore for 10 min. Automated tracking software (Ethovision; Noldus) was used to measure the time spent in the light box and count the number of transitions between the light and dark compartments. Decreased time spent in the light box represents anxiety-like behavior (37). Mice that spent more than 500 s in the light box or made <3 transitions between the light/dark box were removed as this demonstrated aversion to the dark box.

(ii) OFT. General locomotor activity and anxiety-like behavior were assessed using the OFT (36). Briefly, mice were placed in a novel arena (30 by 30 cm) and allowed to explore for 10 min. Locomotor activity was assessed by measuring the total distance traveled (meters). Time spent in the center zone (12 by 12 cm) and the number of transitions into the center zone served as secondary measures of anxiety-like behavior. Automated tracking software (Ethovision; Noldus) was used to measure parameters.

(iii) NOR task. Recognition memory was assessed using the NOR task (36, 38, 39). Mice were placed in an arena (30 by 30 cm) and allowed to acclimate for 10 min. Behavior during the acclimation period was recorded and analyzed as part of the OFT (described above). The NOR task consisted of two phases: training and testing. In the training phase, mice explored two identical objects placed in the arena for 5 min, followed by 45 min of rest in their home cage. During the testing phase, mice were returned to the arena, where one of the familiar objects was replaced with a novel object, and exploratory behavior was recorded for 5 min. The number of interactions with each object in the training and testing phases was scored manually (J. A. Sladek and C. Hennessey), with the exploration ratio calculated as the number of interactions with the new object divided by the total number of interactions. Recognition was determined by increased interaction with the new object versus the familiar object. A decreased exploration ratio indicates a deficit in recognition memory. Only mice that passed recognition criteria (no preference for either object [40 to 60% recognition] during the training phase and at least 10 interactions with both objects in either phase) were included.

Histology. Tissue (distal ileum/proximal colon) was collected at P14 (7 days p.i.) and adulthood (6 to 8 weeks of age) and formalin fixed and paraffined embedded (FFPE). Briefly, tissues were fixed in 10% formalin for at least 48 h, transferred to 70% ethanol, and processed for embedding in paraffin. Blocks were cut using a microtome and transferred onto glass slides (5-μm sections), which were deparaffinized, dehydrated, and stained with hematoxylin and eosin (H&E). Images were taken on a light microscope (Nikon Eclipse E600 microscope using a Nikon DS-U3 digital sight) and quantified for the crypt-villus axis (ileum) (micrometers) and crypt depth (colon) (micrometers) using ImageJ (NIH).

Immunofluorescence. (i) Intestinal epithelial cell proliferation. To characterize the host response to infection, epithelial cell proliferation was assessed at P14 (7 days p.i.) in the distal ileum and proximal colon via immunofluorescence and confocal microscopy (40). FFPE samples were deparaffinized and stained for the cell proliferation marker Ki67 (rabbit anti-Ki67, Alexa Fluor 555 goat anti-rabbit [catalog number A21428; Life Technologies]) and the epithelial cell marker E-cadherin (CDH1) (mouse anti-CDH1 [catalog number CM1681; ECM Biosciences] and streptavidin-Alexa Fluor 647 [catalog number S32357; Invitrogen]) using a mouse-on-mouse (MOM) immunodetection kit (Vector Labs), and nuclei were stained with 4′,6-diamidino-2-phenylindole (DAPI). Confocal images were taken with a 40× objective (SP8; Leica) using a tiling approach, with adjacent images acquired with 10% overlap. Tile scans were stitched and autoscaled (Imaris) to quantify the number of Ki67$^+$ CDH1$^+$ cells per crypt.

(ii) Neurogenesis. Perfused brains were postfixed in 4% PFA (48 h) and cryoprotected in 30% sucrose plus 0.1% sodium azide in phosphate-buffered saline (PBS) at 4°C for at least 48 h. Brains were subsequently embedded in optimal cutting temperature (OCT) medium (Fisher Scientific) and stored at −20°C. Coronal sections (40 μm) were cut using a cryostat (Leica, Germany). Neurogenesis was assessed by quantifying the numbers of proliferating cells (Ki67$^+$) and immature neurons (DCX$^+$) in the DG region of the hippocampus (36). Coronal sections were costained with primary antibodies (rabbit anti-Ki67 [catalog number LS-C141898; Lifespan Biosciences, Seattle, WA] and guinea pig anti-DCX [catalog number AB2253; Millipore, Burlington, MA]), followed by secondary antibodies (Ki67, Alexa Fluor 647 goat anti-rabbit [catalog number ab150155; Abcam, Cambridge, UK]; DCX, Alexa Fluor 555 goat anti-guinea pig [catalog number A21435; Invitrogen]), and nuclei were stained with DAPI. Confocal images were taken with a 20× objective (SP8; Leica) with a 1.04-μm z-step size, with the numbers of Ki67$^+$ and DCX$^+$ cells per DG volume quantified using Imaris (8.2.1) (41) and presented as the number of positive cells per cubic micrometer.

(iii) Neuroinflammation. Microglia morphology was used to assess hippocampal neuroinflammation (19). Coronal brain sections (as described above for neurogenesis studies) were stained with rabbit anti-Iba1 (catalog number 019-19741; Wako), followed by secondary antibody (Alexa Fluor 546 donkey anti-rabbit; Invitrogen) and DAPI for nuclear staining. Confocal images were taken with a 63× objective and 0.3-μm z-steps (SP8; Leica). Three-dimensional (3D) reconstructions of microglia were performed using a modified version of the open-source 3DMorph Matlab script (42) and Imaris software for cell quantification and characterization of processes (length, numbers, and branch points) in both the DG and the CA1 regions to assess microglia morphology and quantify activation (43).

Ussing chambers. The distal ileum and proximal colon were excised, cut along the mesenteric border, and mounted onto cassettes (Physiologic Instruments, San Diego, CA) for Ussing chamber studies (36, 43). Each cassette exposed 0.1 cm^2 of tissue area to 4 ml of circulating oxygenated Ringer's buffer (115 mM NaCl, 1.25 mM CaCl$_2$, 1.2 mM MgCl$_2$, 2.0 mM KH$_2$PO$_4$, and 25 mM NaHCO$_3$ at pH 7.35 ± 0.02 at 37°C). To provide the tissue with energy, 10 mM glucose (Sigma) was added to the serosal compartment, which was osmotically balanced with 10 mM mannitol (ileum) or glucose (colon) in the mucosal compartment. Two pairs of electrodes attached to agar-salt bridges were used to (i) monitor the potential difference (PD) between the mucosal and serosal compartments and (ii) inject current to maintain the PD at zero during voltage clamping. Recordings and current injection were performed using an automated voltage clamp and Acquire and Analyze software

(Physiologic Instruments). After 15 min of equilibration, 4-kDa FITC-labeled dextran (88 mg/ml) (FD4; Sigma) was added to the mucosal chamber to measure macromolecular permeability over time. Baseline active ion transport was measured by short-circuit current (I_{sc}) (microamperes per square centimeter), and tight junction permeability was measured by conductance (G) (millisiemens per square centimeter). Serosal samples were collected every 30 min for 2 h, with FITC-dextran flux (nanograms per milliliter per square centimeter per hour) determined by measuring the FITC concentration on a plate reader (Synergy H1; BioTek). Values that were outside the standard physiological range (1 to 20 mV) (44) were omitted, as were samples with visible FITC in the serosal side, indicating a tear in the tissue preparation.

qPCR. GI (distal ileum and proximal colon) and brain (hippocampus, PFC, and cerebellum) samples were collected and stored in TRIzol (Invitrogen, Carlsbad, CA) at −80°C. RNA was extracted according to the manufacturer's protocol (Invitrogen) and quantified using a Nanodrop spectrophotometer. RNA was reverse transcribed into cDNA using an iScript cDNA transcriptase kit (Bio-Rad). Relative gene expression levels of cytokines, PRRs, and neurotrophic factors were determined by qPCR (QuantStudio 6 Flex; Applied Biosystems) with SYBR green master mix using primers from Primerbank (45) (see Table S1 in the supplemental material). The qPCR cycling conditions included an initial denaturation step at 95°C for 10 min followed by 40 cycles of 95°C for 15 s and 60°C for 30 s and a melt curve. Data were analyzed using the $2^{-\Delta\Delta CT}$ method with β-actin as the reference gene and are presented as fold changes relative to sham-infected controls, which were normalized to 1.0.

Microbiome analysis. Fecal samples were collected at euthanasia, frozen at −80°C, and sent to Molecular Research LLC (MR DNA) for processing and sequencing. DNA was extracted using the PowerSoil fecal extraction kit (Qiagen), with library preparation and sequencing performed using primer pair 515F and 806R in a 300-bp paired-end run on an Illumina MiSeq platform (Illumina, San Diego, CA). Sequencing data were analyzed using QIIME2 version 2019.7.0 (46) with demultiplexed paired-end sequences with barcodes and adapters removed. DADA2 was used for quality filtering and feature (operational taxonomic unit [OTU]) prediction (47). Based on sequence quality, the forward reads were truncated to 220 nucleotides (nt), and the reverse reads were truncated to 230 nt. MAFFT was used to align representative sequences (48), which were organized into a phylogenetic tree using FastTree 2 (49). Taxonomic classification using OTUs/features was performed using a pretrained naive Bayes taxonomy classifier, Silva132_99%OTUs (50), to generate taxonomic counts and percentage (relative frequency) tables. Diversity analyses were run on the resulting OTU/feature.biom tables to provide both phylogenetic and nonphylogenetic metrics of alpha and beta diversity (51).

Statistical analysis. Results are presented as averages ± standard errors of the means (SEM). One-way analysis of variance (ANOVA) (with Holm-Sidak or Tukey *post hoc* analysis) or Student's *t* test (with Welch's correction for unequal variances) and a Mann-Whitney test (nonparametric data) were performed where appropriate using Prism V.9 (GraphPad, San Diego, CA). A Kruskal-Wallis pairwise comparison was used for microbiome analysis for alpha diversity. A *P* value of ≤0.05 was considered to be statistically significant.

Data availability. Raw sequences have been uploaded to the NCBI Sequence Read Archive under accession number PRJNA478451.

SUPPLEMENTAL MATERIAL

Supplemental material is available online only.
SUPPLEMENTAL FILE 1, PDF file, 0.5 MB.

REFERENCES

1. Lanata CF, Fischer-Walker CL, Olascoaga AC, Torres CX, Aryee MJ, Black RE, Child Health Epidemiology Reference Group of the World Organization and UNICEF. 2013. Global causes of diarrheal disease mortality in children <5 years of age: a systematic review. PLoS One 8:e72788. https://doi.org/10.1371/journal.pone.0072788.
2. Donowitz M, Alpers DH, Binder HJ, Brewer T, Carrington J, Grey MJ. 2012. Translational approaches for pharmacotherapy development for acute diarrhea. Gastroenterology 142:e1–e9. https://doi.org/10.1053/j.gastro.2012.01.014.
3. Oria RB, Murray-Kolb LE, Scharf RJ, Pendergast LL, Lang DR, Kolling GL, Guerrant RL. 2016. Early-life enteric infections: relation between chronic systemic inflammation and poor cognition in children. Nutr Rev 74:374–386. https://doi.org/10.1093/nutrit/nuw008.
4. Niehaus MD, Moore SR, Patrick PD, Derr LL, Lorntz B, Lima AA, Guerrant RL. 2002. Early childhood diarrhea is associated with diminished cognitive function 4 to 7 years later in children in a northeast Brazilian shantytown. Am J Trop Med Hyg 66:590–593. https://doi.org/10.4269/ajtmh.2002.66.590.
5. MAL-ED Network Investigators. 2014. The MAL-ED study: a multinational and multidisciplinary approach to understand the relationship between enteric pathogens, malnutrition, gut physiology, physical growth, cognitive development, and immune responses in infants and children up to 2 years of age in resource-poor environments. Clin Infect Dis 59(Suppl 4):S193–S206. https://doi.org/10.1093/cid/ciu653.
6. Semple BD, Blomgren K, Gimlin K, Ferriero DM, Noble-Haeusslein LJ. 2013. Brain development in rodents and humans: identifying benchmarks of maturation and vulnerability to injury across species. Prog Neurobiol 106–107:1–16. https://doi.org/10.1016/j.pneurobio.2013.04.001.
7. Noah TK, Donahue B, Shroyer NF. 2011. Intestinal development and differentiation. Exp Cell Res 317:2702–2710. https://doi.org/10.1016/j.yexcr.2011.09.006.

8. Rodriguez JM, Murphy K, Stanton C, Ross RP, Kober OI, Juge N, Avershina E, Rudi K, Narbad A, Jenmalm MC, Marchesi JR, Collado MC. 2015. The composition of the gut microbiota throughout life, with an emphasis on early life. Microb Ecol Health Dis 26:26050. https://doi.org/10.3402/mehd.v26.26050.

9. Gareau MG. 2016. Cognitive function and the microbiome. Int Rev Neurobiol 131:227–246. https://doi.org/10.1016/bs.irn.2016.08.001.

10. Cryan JF, O'Riordan KJ, Cowan CSM, Sandhu KV, Bastiaanssen TFS, Boehme M, Codagnone MG, Cussotto S, Fulling C, Golubeva AV, Guzzetta KE, Jaggar M, Long-Smith CM, Lyte JM, Martin JA, Molinero-Perez A, Moloney G, Morelli E, Morillas E, O'Connor R, Cruz-Pereira JS, Peterson VL, Rea K, Ritz NL, Sherwin E, Spichak S, Teichman EM, van de Wouw M, Ventura-Silva AP, Wallace-Fitzsimons SE, Hyland N, Clarke G, Dinan TG. 2019. The microbiota-gut-brain axis. Physiol Rev 99:1877–2013. https://doi.org/10.1152/physrev.00018.2018.

11. Leclercq S, Mian FM, Stanisz AM, Bindels LB, Cambier E, Ben-Amram H, Koren O, Forsythe P, Bienenstock J. 2017. Low-dose penicillin in early life induces long-term changes in murine gut microbiota, brain cytokines and behavior. Nat Commun 8:15062. https://doi.org/10.1038/ncomms15062.

12. Gareau MG, Wine E, Rodrigues DM, Cho JH, Whary MT, Philpott DJ, Macqueen G, Sherman PM. 2011. Bacterial infection causes stress-induced memory dysfunction in mice. Gut 60:307–317. https://doi.org/10.1136/gut.2009.202515.

13. Lyte M, Li W, Opitz N, Gaykema RP, Goehler LE. 2006. Induction of anxiety-like behavior in mice during the initial stages of infection with the agent of murine colonic hyperplasia Citrobacter rodentium. Physiol Behav 89:350–357. https://doi.org/10.1016/j.physbeh.2006.06.019.

14. Mackos AR, Galley JD, Eubank TD, Easterling RS, Parry NM, Fox JG, Lyte M, Bailey MT. 2016. Social stress-enhanced severity of Citrobacter rodentium-induced colitis is CCL2-dependent and attenuated by probiotic Lactobacillus reuteri. Mucosal Immunol 9:515–526. https://doi.org/10.1038/mi.2015.81.

15. Silberger DJ, Zindl CL, Weaver CT. 2017. Citrobacter rodentium: a model enteropathogen for understanding the interplay of innate and adaptive components of type 3 immunity. Mucosal Immunol 10:1108–1117. https://doi.org/10.1038/mi.2017.47.

16. Dupont A, Sommer F, Zhang K, Repnik U, Basic M, Bleich A, Kuhnel M, Backhed F, Litvak Y, Fulde M, Rosenshine I, Hornef MW. 2016. Age-dependent susceptibility to enteropathogenic Escherichia coli (EPEC) infection in mice. PLoS Pathog 12:e1005616. https://doi.org/10.1371/journal.ppat.1005616.

17. Johnston ST, Shtrahman M, Parylak S, Goncalves JT, Gage FH. 2016. Paradox of pattern separation and adult neurogenesis: a dual role for new neurons balancing memory resolution and robustness. Neurobiol Learn Mem 129:60–68. https://doi.org/10.1016/j.nlm.2015.10.013.

18. Miranda M, Morici JF, Zanoni MB, Bekinschtein P. 2019. Brain-derived neurotrophic factor: a key molecule for memory in the healthy and the pathological brain. Front Cell Neurosci 13:363. https://doi.org/10.3389/fncel.2019.00363.

19. Erny D, Hrabě de Angelis AL, Jaitin D, Wieghofer P, Staszewski O, David E, Keren-Shaul H, Mahlakoiv T, Jakobshagen K, Buch T, Schwierzeck V, Utermöhlen O, Chun E, Garrett WS, McCoy KD, Diefenbach A, Staeheli P, Stecher B, Amit I, Prinz M. 2015. Host microbiota constantly control maturation and function of microglia in the CNS. Nat Neurosci 18:965–977. https://doi.org/10.1038/nn.4030.

20. Abdel-Haq R, Schlachetzki JCM, Glass CK, Mazmanian SK. 2019. Microbiome-microglia connections via the gut-brain axis. J Exp Med 216:41–59. https://doi.org/10.1084/jem.20180794.

21. Das S, Jayaratne R, Barrett KE. 2018. The role of ion transporters in the pathophysiology of infectious diarrhea. Cell Mol Gastroenterol Hepatol 6:33–45. https://doi.org/10.1016/j.jcmgh.2018.02.009.

22. Heijtz RD, Wang S, Anuar F, Qian Y, Bjorkholm B, Samuelsson A, Hibberd ML, Forssberg H, Pettersson S. 2011. Normal gut microbiota modulates brain development and behavior. Proc Natl Acad Sci U S A 108:3047–3052. https://doi.org/10.1073/pnas.1010529108.

23. Neufeld KM, Kang N, Bienenstock J, Foster JA. 2011. Reduced anxiety-like behavior and central neurochemical change in germ-free mice. Neurogastroenterol Motil 23:255–264, e119. https://doi.org/10.1111/j.1365-2982.2010.01620.x.

24. Frohlich EE, Farzi A, Mayerhofer R, Reichmann F, Jacan A, Wagner B, Zinser E, Bordag N, Magnes C, Frohlich E, Kashofer K, Gorkiewicz G, Holzer P. 2016. Cognitive impairment by antibiotic-induced gut dysbiosis: analysis of gut microbiota-brain communication. Brain Behav Immun 56:140–155. https://doi.org/10.1016/j.bbi.2016.02.020.

25. Desbonnet L, Clarke G, Traplin A, O'Sullivan O, Crispie F, Moloney RD, Cotter PD, Dinan TG, Cryan JF. 2015. Gut microbiota depletion from early adolescence in mice: implications for brain and behaviour. Brain Behav Immun 48:165–173. https://doi.org/10.1016/j.bbi.2015.04.004.

26. Bercik P, Verdu EF, Foster JA, Macri J, Potter M, Huang X, Malinowski P, Jackson W, Blennerhassett P, Neufeld KA, Lu J, Khan WI, Corthesy-Theulaz I, Cherbut C, Bergonzelli GE, Collins SM. 2010. Chronic gastrointestinal inflammation induces anxiety-like behavior and alters central nervous system biochemistry in mice. Gastroenterology 139:2102–2112.e1. https://doi.org/10.1053/j.gastro.2010.06.063.

27. Gareau MG, Jury J, MacQueen G, Sherman PM, Perdue MH. 2007. Probiotic treatment of rat pups normalises corticosterone release and ameliorates colonic dysfunction induced by maternal separation. Gut 56:1522–1528. https://doi.org/10.1136/gut.2006.117176.

28. De Palma G, Blennerhassett P, Lu J, Deng Y, Park AJ, Green W, Denou E, Silva MA, Santacruz A, Sanz Y, Surette MG, Verdu EF, Collins SM, Bercik P. 2015. Microbiota and host determinants of behavioural phenotype in maternally separated mice. Nat Commun 6:7735. https://doi.org/10.1038/ncomms8735.

29. Baptista P, Andrade JP. 2018. Adult hippocampal neurogenesis: regulation and possible functional and clinical correlates. Front Neuroanat 12:44. https://doi.org/10.3389/fnana.2018.00044.

30. Mirescu C, Peters JD, Gould E. 2004. Early life experience alters response of adult neurogenesis to stress. Nat Neurosci 7:841–846. https://doi.org/10.1038/nn1290.

31. Ogbonnaya ES, Clarke G, Shanahan F, Dinan TG, Cryan JF, O'Leary OF. 2015. Adult hippocampal neurogenesis is regulated by the microbiome. Biol Psychiatry 78:e7–e9. https://doi.org/10.1016/j.biopsych.2014.12.023.

32. Bland ST, Beckley JT, Young S, Tsang V, Watkins LR, Maier SF, Bilbo SD. 2010. Enduring consequences of early-life infection on glial and neural cell genesis within cognitive regions of the brain. Brain Behav Immun 24:329–338. https://doi.org/10.1016/j.bbi.2009.09.012.

33. Petri WA, Jr, Miller M, Binder HJ, Levine MM, Dillingham R, Guerrant RL. 2008. Enteric infections, diarrhea, and their impact on function and development. J Clin Invest 118:1277–1290. https://doi.org/10.1172/JCI34005.

34. Sturgeon JP, Bourke CD, Prendergast AJ. 2019. Children with noncritical infections have increased intestinal permeability, endotoxemia and altered innate immune responses. Pediatr Infect Dis J 38:741–748. https://doi.org/10.1097/INF.0000000000002311.

35. Rincel M, Aubert P, Chevalier J, Grohard PA, Basso L, Monchaux de Oliveira C, Helbling JC, Levy E, Chevalier G, Leboyer M, Eberl G, Laye S, Capuron L, Vergnolle N, Neunlist M, Boudin H, Lepage P, Darnaudery M. 2019. Multi-hit early life adversity affects gut microbiota, brain and behavior in a sex-dependent manner. Brain Behav Immun 80:179–192. https://doi.org/10.1016/j.bbi.2019.03.006.

36. Pusceddu MM, Barboza M, Keogh CE, Schneider M, Stokes P, Sladek JA, Kim HJD, Torres-Fuentes C, Goldfild LR, Gillis SE, Brust-Mascher I, Rabasa G, Wong KA, Lebrilla C, Byndloss MX, Maisonneuve C, Baumler AJ, Philpott DJ, Ferrero RL, Barrett KE, Reardon C, Gareau MG. 2019. Nod-like receptors are critical for gut-brain axis signalling in mice. J Physiol 597:5777–5797. https://doi.org/10.1113/JP278640.

37. Bourin M, Hascoet M. 2003. The mouse light/dark box test. Eur J Pharmacol 463:55–65. https://doi.org/10.1016/s0014-2999(03)01274-3.

38. Smith CJ, Emge JR, Berzins K, Lung L, Khamishon R, Shah P, Rodrigues DM, Sousa AJ, Reardon C, Sherman PM, Barrett KE, Gareau MG. 2014. Probiotics normalize the gut-brain-microbiota axis in immunodeficient mice. Am J Physiol Gastrointest Liver Physiol 307:G793–G802. https://doi.org/10.1152/ajpgi.00238.2014.

39. Emge JR, Huynh K, Miller EN, Kaur M, Reardon C, Barrett KE, Gareau MG. 2016. Modulation of the microbiota-gut-brain axis by probiotics in a murine model of inflammatory bowel disease. Am J Physiol Gastrointest Liver Physiol 310:G989–G998. https://doi.org/10.1152/ajpgi.00086.2016.

40. Ramirez VT, Godinez DR, Brust-Mascher I, Nonnecke EB, Castillo PA, Gardner MB, Tu D, Sladek JA, Miller EN, Lebrilla CB, Bevins CL, Gareau MG, Reardon C. 2019. T-cell derived acetylcholine aids host defenses during enteric bacterial infection with Citrobacter rodentium. PLoS Pathog 15:e1007719. https://doi.org/10.1371/journal.ppat.1007719.

41. O'Leary OF, Ogbonnaya ES, Felice D, Levone BR, Conroy LC, Fitzgerald P, Bravo JA, Forsythe P, Bienenstock J, Dinan TG, Cryan JF. 2018. The vagus nerve modulates BDNF expression and neurogenesis in the hippocampus. Eur Neuropsychopharmacol 28:307–316. https://doi.org/10.1016/j.euroneuro.2017.12.004.

42. York EM, LeDue JM, Bernier L-P, MacVicar BA. 2018. 3DMorph automatic analysis of microglial morphology in three dimensions from ex vivo and

in vivo imaging. eNeuro 5:ENEURO.0266-18.2018. https://doi.org/10 .1523/ENEURO.0266-18.2018.

43. Salvo E, Stokes P, Keogh CE, Brust-Mascher I, Hennessey C, Knotts TA, Sladek JA, Rude KM, Swedek M, Rabasa G, Gareau MG. 2020. A murine model of pediatric inflammatory bowel disease causes microbiota-gut-brain axis deficits in adulthood. Am J Physiol Gastrointest Liver Physiol 319:G361–G374. https://doi.org/10.1152/ajpgi.00177.2020.

44. Clarke LL. 2009. A guide to Ussing chamber studies of mouse intestine. Am J Physiol Gastrointest Liver Physiol 296:G1151–G1166. https://doi.org/10 .1152/ajpgi.90649.2008.

45. Wang X, Spandidos A, Wang H, Seed B. 2012. PrimerBank: a PCR primer database for quantitative gene expression analysis, 2012 update. Nucleic Acids Res 40:D1144–D1149. https://doi.org/10.1093/nar/gkr1013.

46. Bolyen E, Rideout JR, Dillon MR, Bokulich NA, Abnet CC, Al-Ghalith GA, Alexander H, Alm EJ, Arumugam M, Asnicar F, Bai Y, Bisanz JE, Bittinger K, Brejnrod A, Brislawn CJ, Brown CT, Callahan BJ, Caraballo-Rodríguez AM, Chase J, Cope EK, Da Silva R, Diener C, Dorrestein PC, Douglas GM, Durall DM, Duvallet C, Edwardson CF, Ernst M, Estaki M, Fouquier J, Gauglitz JM, Gibbons SM, Gibson DL, Gonzalez A, Gorlick K, Guo J, Hillmann B, Holmes S, Holste H, Huttenhower C, Huttley GA, Janssen S, Jarmusch AK, Jiang L, Kaehler BD, Kang KB, Keefe CR, Keim P, Kelley ST, Knights D, et al. 2019. Reproducible, interactive, scalable and extensible microbiome data science using QIIME 2. Nat Biotechnol 37:852–857. https://doi.org/10.1038/ s41587-019-0209-9.

47. Callahan BJ, McMurdie PJ, Rosen MJ, Han AW, Johnson AJ, Holmes SP. 2016. DADA2: high-resolution sample inference from Illumina amplicon data. Nat Methods 13:581–583. https://doi.org/10.1038/nmeth.3869.

48. Katoh K, Standley DM. 2013. MAFFT multiple sequence alignment software version 7: improvements in performance and usability. Mol Biol Evol 30:772–780. https://doi.org/10.1093/molbev/mst010.

49. Price MN, Dehal PS, Arkin AP. 2010. FastTree 2—approximately maximum-likelihood trees for large alignments. PLoS One 5:e9490. https://doi .org/10.1371/journal.pone.0009490.

50. Quast C, Pruesse E, Yilmaz P, Gerken J, Schweer T, Yarza P, Peplies J, Glockner FO. 2013. The SILVA ribosomal RNA gene database project: improved data processing and Web-based tools. Nucleic Acids Res 41: D590–D596. https://doi.org/10.1093/nar/gks1219.

51. Lozupone C, Lladser ME, Knights D, Stombaugh J, Knight R. 2011. UniFrac: an effective distance metric for microbial community comparison. ISME J 5:169–172. https://doi.org/10.1038/ismej.2010.133.